

YOLOv8 for Defect Inspection of Hexagonal Directed Self-Assembly Patterns: A Data-Centric Approach

Enrique Dehaerne^{a,b}, Bappaditya Dey^b, Hossein Esfandiar^{c,b}, Lander Verstraete^b, Hyo Seon Suh^b, Sandip Halder^b, and Stefan De Gendt^{a,b}

^aFaculty of Science, KU Leuven, 3001 Leuven, Belgium

^bInteruniversity Microelectronics Centre (imec), 3001 Leuven, Belgium

^cDept. of Chemistry, Materials and Chemical Engineering, Giulio Natta; Politecnico di Milano; I-20133 Milano; Italy

ABSTRACT

Shrinking pattern dimensions leads to an increased variety of defect types in semiconductor devices. This has spurred innovation in patterning approaches such as Directed self-assembly (DSA) for which no traditional, automatic defect inspection software exists. Machine Learning-based SEM image analysis has become an increasingly popular research topic for defect inspection with supervised ML models often showing the best performance. However, little research has been done on obtaining a dataset with high-quality labels for these supervised models. In this work, we propose a method for obtaining coherent and complete labels for a dataset of hexagonal contact hole DSA patterns while requiring minimal quality control effort from a DSA expert. We show that YOLOv8, a state-of-the-art neural network, achieves defect detection precisions of more than 0.9 mAP on our final dataset which best reflects DSA expert defect labeling expectations. We discuss the strengths and limitations of our proposed labeling approach and suggest directions for future work in data-centric ML-based defect inspection.

Keywords: Semiconductor defect inspection, machine learning, deep learning, object detection, YOLOv8, supervised learning, data-centric learning, directed self-assembly

1. INTRODUCTION

Shrinking semiconductor pattern dimensions has led to increased manufacturing complexity. This complexity has led to a greater number of stochastic defects to inspect. Scanning Electron Microscopy (SEM) is a workhorse fab tool since it can image at high resolution relatively fast. However, SEM images are inherently noisy. Capturing too many frames to reduce this noise can cost time and can be destructive for materials to be inspected such as thin resists. Machine Learning (ML)-based defect detection methods for SEM images are becoming a popular research topic due to their ability to deal with noise better than conventional image processing algorithms.¹ Additionally, ML-based methods are more easily adaptable to pattern changes (e.g. CD/Pitch variation) and imaging conditions (contrast, field-of-view, etc.). Supervised learning, where an ML model learns by comparing its predictions against (pseudo-)ground truth labels (generally defined by a human expert), usually leads to the best performance. However, the performance of supervised learning depends on the quality of the labels provided by a human labeler.

In this study, we apply the latest object detection model of the popular YOLO² (You Only Look Once) family, YOLOv8,³ to detect challenging defects in Hexagonal Directed self-assembly (DSA) patterns. Hexagonal DSA patterns make for an interesting case study as they can contain unique defects that traditional defect inspection software cannot detect or classify. We investigate the effect of variance between human labelers. We consider three labeled datasets, each containing the same SEM images labeled by different human labelers. We propose a data-centric approach to combine labels from multiple labelers and align them with DSA expert expectations. We show that training YOLOv8 models on this final, combined dataset results in detection performance that best matches DSA expert expectations.

Send correspondence to Enrique Dehaerne, e-mail: enrique.dehaerne@imec.be

2. RELATED WORK

2.1 Data-centric ML

Data-centric ML refers to improving an ML system’s performance by enhancing the dataset used to train a given model.⁴ This stands in contrast to the model-centric ML approach which, for a given dataset that is assumed to be fixed, makes changes to the ML model to improve the performance of the system. Broadly, methods for data collection/curation,^{5,6} preparation/augmentation,^{7,8} and labeling^{9,10} can all be considered as data-centric improvements for ML systems.

2.2 Semiconductor defect inspection

Traditionally, semiconductor defect inspection uses hand-crafted image-processing algorithms.^{11–13} While these algorithms typically perform well for specific inspection scenarios, they struggle to adapt to variations in patterns and imaging conditions. Defect inspection for DSA patterning has been studied using more traditional techniques.^{14–16} To the best of our knowledge, no ML-based approaches for defect inspection of DSA patterns have been published. ML-based SEM defect detection methods, especially Convolutional Neural Network (CNN) models, are becoming popular due to their improved robustness to these variations. Two main paradigms for training defect inspection models exist, supervised^{1,17–19} and unsupervised^{20–22} learning. Supervised learning, where an ML model learns by comparing its predictions to labels provided by a human expert, usually leads to the best performance for defect detection and classification. Note, the performance of supervised learning depends on the quality of the labels. The majority of data-centric works in the semiconductor defect inspection domain have focused on data augmentation techniques.^{23,24} In this study, we propose improving label quality as another method for improving the performance of CNN-based semiconductor defect detection systems.

3. HEXAGONAL DIRECTED SELF-ASSEMBLY SEM IMAGE DATASET

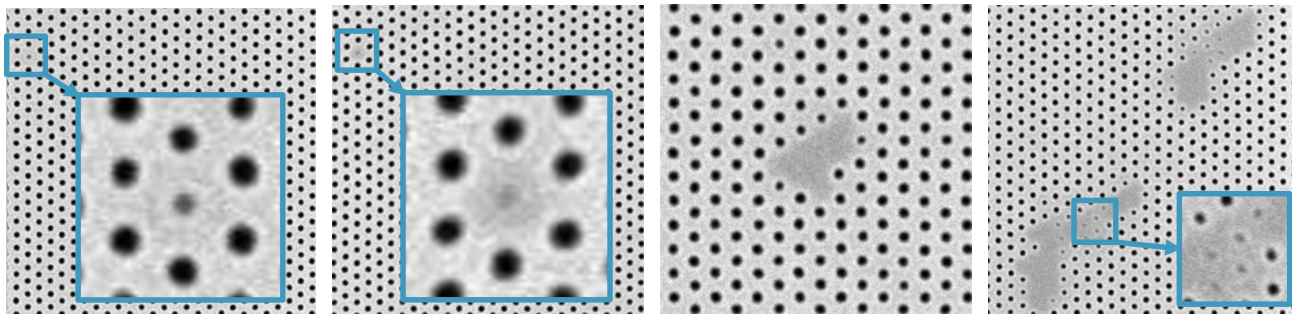
For this research work, we collected a novel dataset of hexagonal DSA SEM images with defects. DSA is a patterning technique that uses the inherent period of block-copolymer (BCP) materials to define line/space or hexagonal hole patterns from the bottom up.^{25,26} To generate well-aligned patterns, a guiding pattern for the BCP materials is needed. While this guiding pattern is typically created by conventional lithography techniques, the final pattern characteristics are defined by the self-assembled BCP materials. This allows DSA to overcome stochastic issues commonly associated with EUV lithography. However, DSA is known to have specific defects that are otherwise not observed in conventional lithography patterns. These DSA specific defects are associated with the dynamic processes underlying the self-assembly process. Typical DSA specific defects are dislocations in line/space patterns, which represent a kinetically trapped metastable structure.^{16,27} Similarly, HEXagonal Contact Hole (HEXCH) arrays may suffer from misaligned domains and even non-vertically oriented structures. When etching the latter into the underlying hard mask, closed holes may be observed.

Our novel dataset consists of SEM images of HEXCH DSA pattern defects after etch into a SiN layer. In these images, we localize (in the form of bounding boxes) and classify three different classes of defects. These defect classes are Partially Closed Holes (PCH), Missing Holes (MH), and Closed Patches (CP). PCH and MH defects each relate to one hole while a CP defect relates to a contiguous area of closed holes. As DSA HEXCH patterns are not yet routinely considered in the semiconductor industry, defects in these patterns are not covered in traditional inspection methodology. The DSA dataset images were collected by a DSA patterning expert. The expert inspected each image and partitioned the collection into four sub-collections based on the defects shown in each image. The names given to these partitions correspond to the three defect classes listed above (PCH, MH, and CP) as well as a Multiple Defect (MD) sub-collection. These MD images contained more than one defect of one or more different defect classes. Figure 1 shows examples of defects of these four partitions. The full dataset organized into these four sub-collections was given to three different labelers with instructions to draw and classify bounding boxes that best capture the extent of each defect in each image. In the rest of this paper we refer to the labelers as *labeler A*, *labeler B*, and *labeler C*. Note that this initial partitioning of the dataset is not necessary for the labeling methodology proposed in Section 4.

The dataset was randomly split into train, validation, and test subsets with a ratio of 70:15:15, respectively. The image-level statistics of the dataset are provided in Table 1. Each SEM image has a resolution of 1000×1000 pixels.

Table 1: SEM image counts for each split and partition of the HEXCH DSA dataset.

Partition	Train	Validation	Test	All
Partially Closed Hole (PCH)	73	13	18	104
Missing Hole (MH)	29	8	5	42
Closed Patch (CP)	72	13	19	104
Multiple Defect (MD)	63	17	9	89
Total	237	51	51	339



(a) Partially Closed Hole (PCH) (b) Missing Hole (MH) (c) Closed Patch (CP) (d) Multiple Defect (MD)

Figure 1: Defect examples for each raw image partition of the full hexagonal DSA dataset. The images are cropped (and zoomed in where necessary).

4. METHODOLOGY

4.1 Semi-automated labeler consensus

To mitigate individual labeler errors and biases, we propose a semi-automated method for combining labels from multiple labelers. A naive method for combining multiple labeled datasets would be to have a DSA expert manually compare labels for each image and remove or modify each label individually. This naive method is inefficient for two main reasons. First, a majority of labels will most likely have consensus in the sense that many labels between multiple labelers overlap to a high degree and are classified as the same class. Second, misunderstanding labeling instructions may lead to common patterns of erroneous labels. Oftentimes, these common patterns can be easily identifiable and automatically corrected without requiring a DSA expert’s manual intervention. To mitigate these inefficiencies, respectively, our proposed method includes: (i) using voting for reclassification and Weighted-Box-Fusion (WBF)²⁸ for bounding box extent to combine overlapping labels and (ii) programmatically correcting common labeling error patterns as identified by a DSA expert. In this way, the proposed method only requires DSA expert intervention two times: (a) breaking ties between labelers during reclassification voting and (b) identifying common erroneous label patterns.

Figure 2 shows a flowchart of the proposed labeling procedure. First, the raw SEM image dataset is labeled by

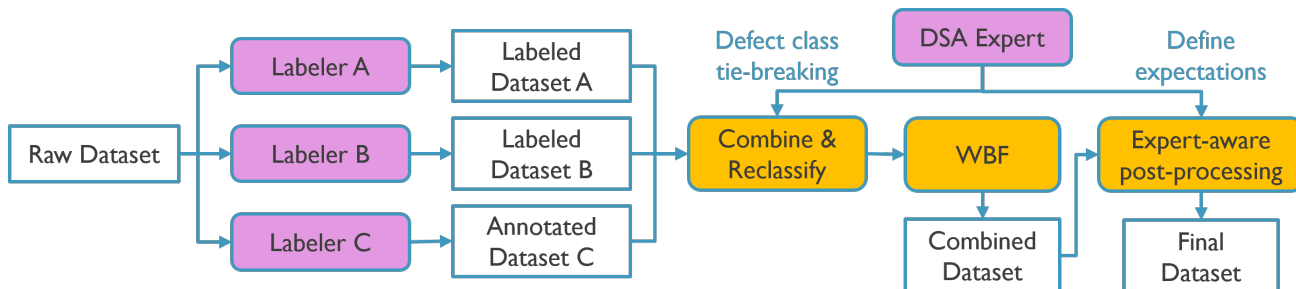
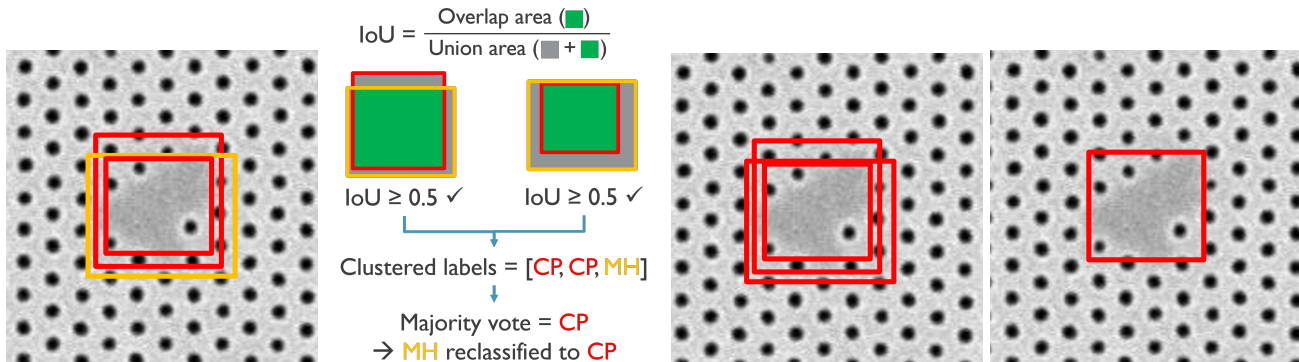


Figure 2: Flowchart of the proposed labeling and consensus methodology.



(a) Example labels for a de- (b) IoU calculation for overlap- (c) IoU calculation for over- (d) Example labels after
fect. ping labels. lapping labels. WBF.

Figure 3: An example scenario with three overlapping labels, two CP labels and one MH label, (3a). Using the orange label as a randomly selected starting label, the labels are clustered together based on having IoU values greater or equal to 0.5 (3b). The most common class in this label cluster is CP so the MH label is changed to a CP label (3b and 3c). The cluster of labels is then fused into a single label using the WBF algorithm (3d).

multiple labelers (three labelers in the case of this study) to obtain multiple labeled datasets. Note that this part does not require any consensus between the labelers which means each labeler can work independently and in parallel, optimizing labeling speed. The labels of all the labelers are then combined on all corresponding images. Standard labeling software was used by the labelers. LabelImg²⁹ was used by labelers B and C. Coco-annotator³⁰ was used by labeler A.

Second, overlapping clusters of labels are reclassified based on voting between these labels. A cluster of labels is formed by selecting a label and adding all other labels in the image that have an Intersection-over-Union (IoU) value greater or equal to 0.5 to a cluster along with the selected label. This is similar to how the WBF algorithm clusters labels to be fused together. Within a cluster, a vote is performed using each label’s class. All labels in the cluster are then reclassified to the class with the most votes. Reclassification vote ties are resolved manually by a DSA expert.

The (possibly reclassified) overlapping clusters of labels are fused into one label via WBF. The WBF algorithm expects as input a list of bounding boxes, each with corresponding labels and confidence scores. Compared to other bounding-box filtering methods such as Non-Maximum Suppression (NMS), WBF does not rely on bounding-boxes having varying confidence scores. This means that we can assign the same confidence score, 1, to all labels since we do not know the confidence of a label. Additionally, WBF has the desirable property that it forms a new bounding box using properties from all boxes in a cluster rather than simply throwing away boxes such as with NMS. After WBF is applied, a *combined dataset* is obtained which can more easily be inspected by a DSA expert than the raw combined labels of all labelers. Figure 3 shows an example of how labels are analyzed for overlap, reclassified via voting, and fused using WBF. The combined dataset is obtained after WBF has been applied to all images of the dataset results in the *combined* dataset.

While it is possible to let the DSA expert thoroughly inspect and correct each label instance of the *combined* dataset, we find that a majority of the labeling errors follow a pattern that the DSA expert can identify by only inspecting a few labeled image samples from the combined dataset. We also find that these common label error patterns can be corrected using automatic post-processing, mitigating the need for the DSA expert to correct these errors manually. The exact required post-processing steps will be different for different labelers and different datasets. The post-processing steps used in our study are discussed in Section 5.1. If very few errors are found, it will most likely be faster to correct these individually. As with all steps in the proposed methodology, using post-processing for error correction scales better with dataset size and erroneous label counts compared to manual label correction.

Following the methodology described above, three datasets labeled by individual labelers (*labelers A, B, and C*) and two labeled datasets from combining and processing these three datasets (*combined* and *final*,

respectively) were obtained. The final dataset is considered to be the labeled dataset most similar to the DSA expert’s ideal dataset. The defect detection performance results on the final dataset are therefore considered to be the most important.

4.2 YOLOv8 defect detection model

The original YOLO model² was developed to achieve a good trade-off between detection performance and inference speed. This is a very desirable characteristic for industrial image-based defect inspection applications where throughput is important. YOLOv8³ is a recent YOLO-style, single-stage object detection model that has been shown to outperform previous YOLO models in terms of mean Average Precision (mAP) on the COCO dataset.³¹ YOLOv8 comes in five different size variants: *nano*, *small*, *medium*, *large*, and *extra-large*. In our experiments, we train, validate, and test each variant on the various labeled datasets obtained from the labeling methodology proposed in the previous subsection. We report the average test results over all of the variants to obtain our final AP results. No consistent differences between model size variants were observed for the experiments conducted.

All experiments were run on a Tesla V100 GPU with 32GB of VRAM unless mentioned otherwise. Images were resized to the closest multiple of 32, 992×992 , since YOLOv8 models have a maximum stride of 32. A batch size of 32 was used for the *nano*, *small*, and *medium* YOLOv8 model variants. A batch size of 16 was used for the *large* and *extra-large* variants. All models were trained for a maximum of 200 epochs. The checkpoint that achieves the best fitness value ($fitness = 0.1 \times mAP@0.5 + 0.9 \times mAP@0.5 : 0.95$), as calculated at the end of each epoch, was used for evaluation. The training for all experiments was automatically stopped if the fitness value did not improve after 50 epochs. All other hyperparameters were kept the same as the default settings of the YOLOv8 GitHub repository.³ Most training runs were completed within 2 hours.

5. RESULTS & DISCUSSION

5.1 Differences in labeled datasets

Figure 4 shows examples of prominent labeling behavior differences between the three labelers. The labeling differences in each row and how these differences were handled are described below:

1. The first row shows labeler A missing or not considering certain holes to be partially closed when labeler B does. Combining labels from all the labelers ensures that as few defects as possible are missed in the final labeled dataset. The first row also shows labeler C wrongly classifying all defects in the MD partition as a separate MD defect class. This is corrected through class voting. For example, in this particular instance, the label from labeler C would be reclassified as a CP since it is the majority vote when considering the overlapping labels from the three labelers.
2. The exact extent of closed patches bounding boxes is different between the three labels in the second row. This is solved by using WBF to fuse the labels into a single label of the same class that has an extent somewhere between all the overlapping labels.
3. The third row shows labelers B and C did not consider labeling partially closed and missing holes instances inside of a closed patch instance separately, while labeler A labeled all of these instances separately. While the image features captured by labeler A’s labels may very well reflect true MH or PCH defect instances, the DSA expert preferred B and C’s labeling. Therefore, for the final dataset, all combined image labels were processed to remove MH and PCH labels within CP labels.
4. The last row again shows some of the labeling differences from the previous row but also shows irregularly shaped closed patches that were broken up into multiple bounding boxes by each labeler differently. While these multiple boxes more precisely encapsulate CP features without capturing non-defective background features, the DSA expert preferred them to be labeled as one CP instead of multiple, separate CPs. For the final dataset, combined image labels were processed to combine overlapping CPs (in this case using an IoU threshold of more than zero) into the smallest box that completely covers all overlapping CPs labels. For this post-processing step, we use an IoU threshold of 0.0001 since most of these adjacent CP boxes barely overlap.

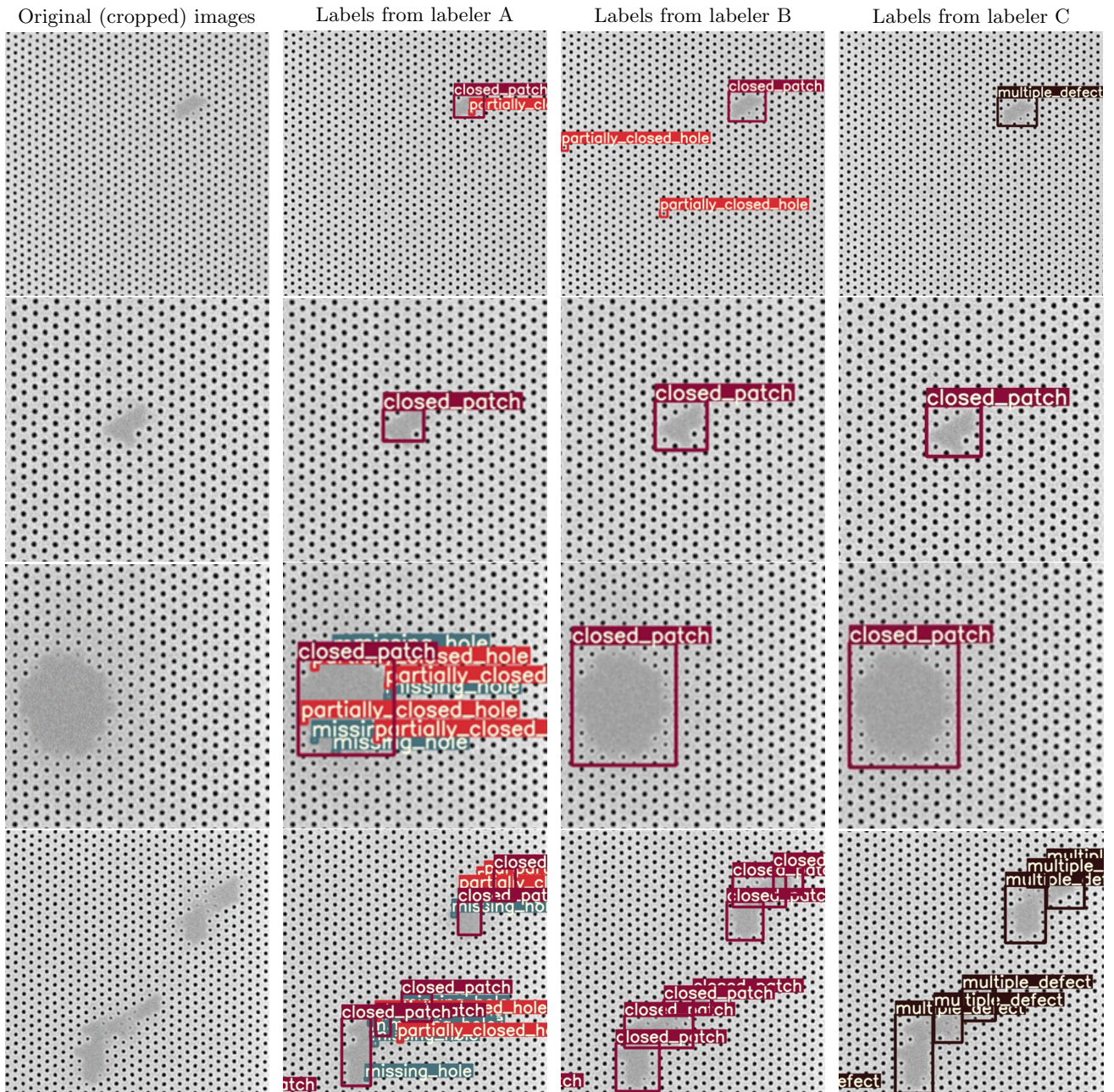


Figure 4: Examples of labeling differences between labelers A, B, and C.

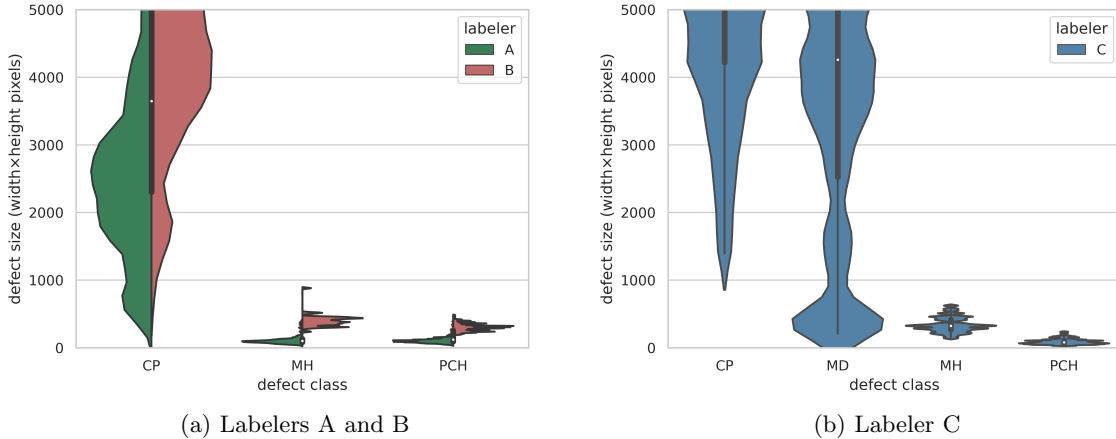


Figure 5: Violin plots for the defect size of labels of the three individually labeled datasets. Each violin is scaled to have the same width. The plots are cut off at a defect size of 5000 to improve readability.

After combining and labeling class voting, MD labels that did not overlap with labels from labelers A or B still remained. As can be seen in Figure 5, the sizes of CP, MH, and PCH labels for labeler C were particularly well separable. Therefore, the remaining MD labels were reclassified to be CPs if their size was larger than the largest MH or PCH label from labelers C. Otherwise, the remaining MDs were reclassified to be PCHs. This was done because the sizes of the remaining MD labels were much more similar to the average size of labeler C’s PCH labels. It can be assumed that PCH labels are more easily to be accidentally missed by labelers than MH labels which further motivated the choice to reclassify the remaining MDs as PCHs instead of MHs.

Figure 6 shows corresponding combined and final dataset labels for the examples shown in Figure 4. It can be seen that the combined dataset contains far more labels than the final dataset. This is confirmed in Figure 7a which shows label count statistics for all images in each labeled dataset. Figure 7b shows the counts for all images except for MD images. The differences in label counts between datasets in Figure 7a are greater than those in Figure 7b which shows that most differences in labeling happen in MD images. We investigate the effects of training and evaluating with/without MD images, which have the highest likelihood to have erroneous labels due to the disagreement between labelers, in the next subsection.

5.2 YOLOv8 defect detection performance

First, we investigate the performance of YOLOv8 models trained and tested only on the individual labeler datasets. Table 2 shows the results of all combinations of train and test datasets from the three labelers. These results show that models trained and evaluated on data from the same labeler (A or B, not C due to the bad classification of MD labels) perform relatively well. Labeler C is an exception for this due to the model’s classification confusion due to the erroneous MD labels. This behavior can be seen in the last row of Figure 8. The results from models trained on data from one labeler and tested on another labeler are significantly worse (again, when ignoring effects from MD labels). This shows that differences in labeling have a significant impact on model performance. The biggest differences are in the cross-labeler results involving labeler A since their label count was far greater than labelers B and C (see Figure 7a) which led to many false positive predictions compared to labeler B or C’s test labels. This behavior can also be seen in Figure 8.

Second, we investigate the performance of models trained and/or tested on the combined and final datasets. Table 3 shows the test results for all of these experiments. Similar to Table 2, we find that the best results come from models trained and evaluated on the same labels. The models trained on the final training data achieved the best result on the target test data, the test final dataset, of 0.919 mAP. This is the third-best overall mAP score achieved. The best overall mAP of 0.944 is achieved by the models trained on the final dataset without MD images and tested on the same data distribution. This suggests that our labeling combination and processing method is more coherent and complete than relying on individual labelers. The MD images are the

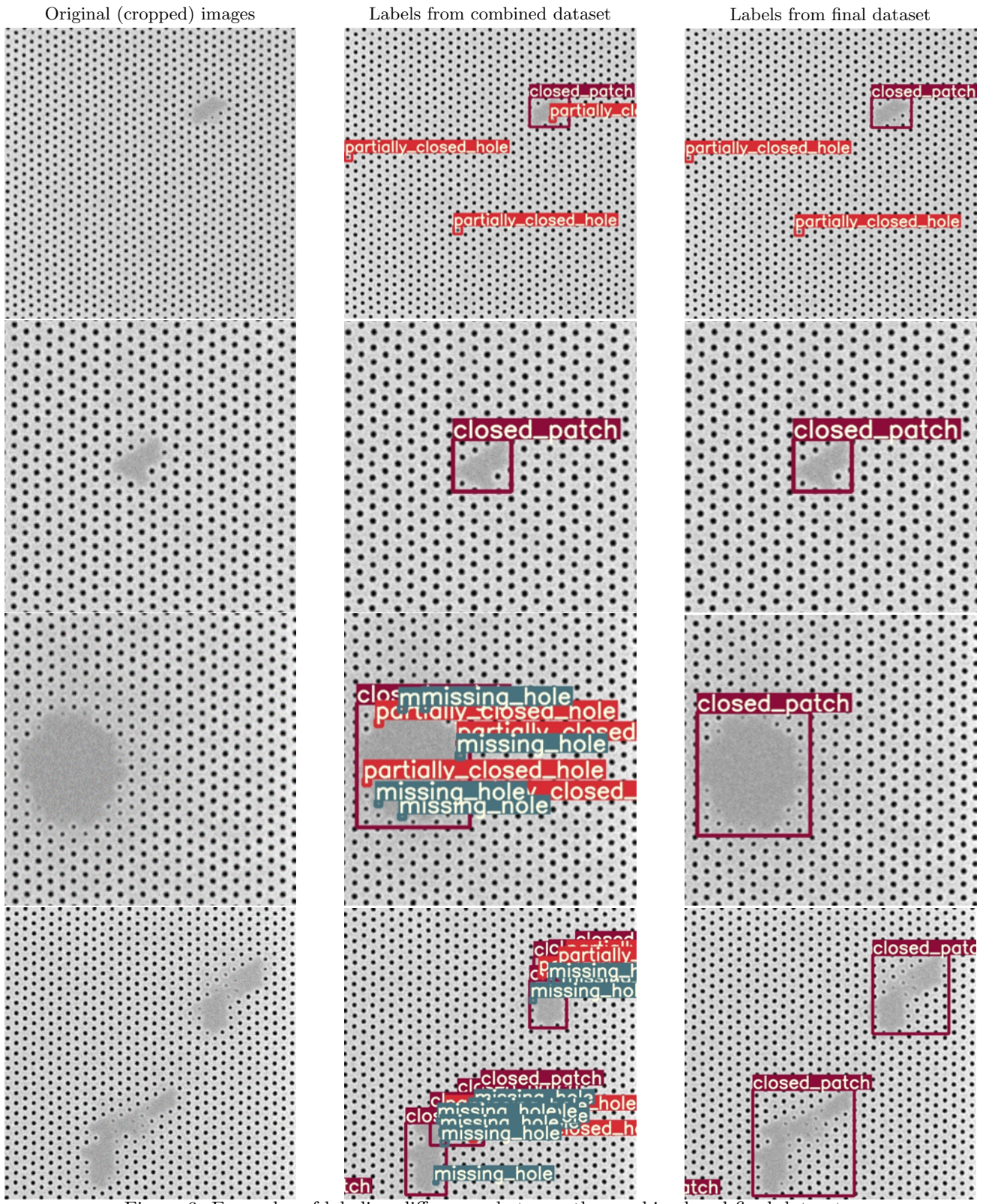


Figure 6: Examples of labeling differences between the combined and final datasets.

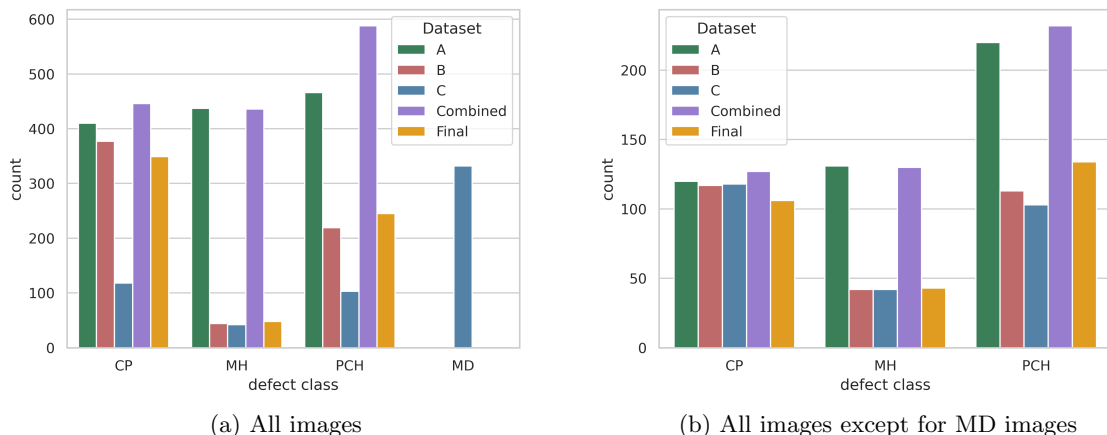


Figure 7: Label counts for each labeled dataset.

Table 2: Per-class AP and mAP results for models trained and tested on datasets labeled by individual labelers. These results are the average of all YOLOv8 size variants. The first three rows of results use models that were trained and validated using the labels of one labeler and tested on the labels of the same labeler. The following rows use labels from different labelers for training and testing.

Labeler		AP (@0.5 IoU)				
train	test	CP	MH	PCH	MD	All (mAP)
A	A	0.883	0.873	0.769	–	0.842
B	B	0.986	0.968	0.765	–	0.906
C	C	0.421	0.716	0.213	0.576	0.482
A	B	0.632	0.072	0.020	–	0.260
	C	0.396	0.052	0.231	0.0	0.226
B	A	0.504	0.096	0.020	–	0.207
	C	0.975	0.796	0.186	0.0	0.652
C	A	0.418	0.079	0.297	–	0.265
	B	0.975	0.804	0.195	–	0.658

most challenging which explains why the test results were better when the models are tested without them. Interestingly, however, models trained on the final dataset without MD images outperformed models trained with MD images for the CP and MH defect classes when tested using MD images (see red values in Figure 3). This suggests that the final labels for the MD images are still a bit noisy. On the other hand, the improved performance of the PCH class when trained on MD images suggests that the optimal training dataset for the models should have a balance between label quality and quantity.

We find that the performance of PCH detection, the most challenging defect class overall, improves most when trained on final dataset labels compared to training on individual labeler data. We also find that the performance of PCH detection increases significantly when no MD images are considered for testing. This could be indicative of false positive PCH labels in the final dataset (especially in MD images) due to the somewhat ambiguous characteristic of PCH defects. An example of such an erroneous label could be the PCH label just below the center of the input image from Figure 8 where only labeler B, potentially erroneously, labeled this defect. Figure 9 shows that models trained on the combined or final datasets did not predict this defect at all.

The models trained on labeler A’s dataset perform decently well on the combined test dataset and poorly on the final dataset. The opposite is true for models trained on labeler B and C’s datasets which perform better on the final dataset than the combined dataset. This is because many of the labels in the combined dataset come exclusively from labeler A.

Applying the same post-processing steps used to create the final dataset to the predictions of the model

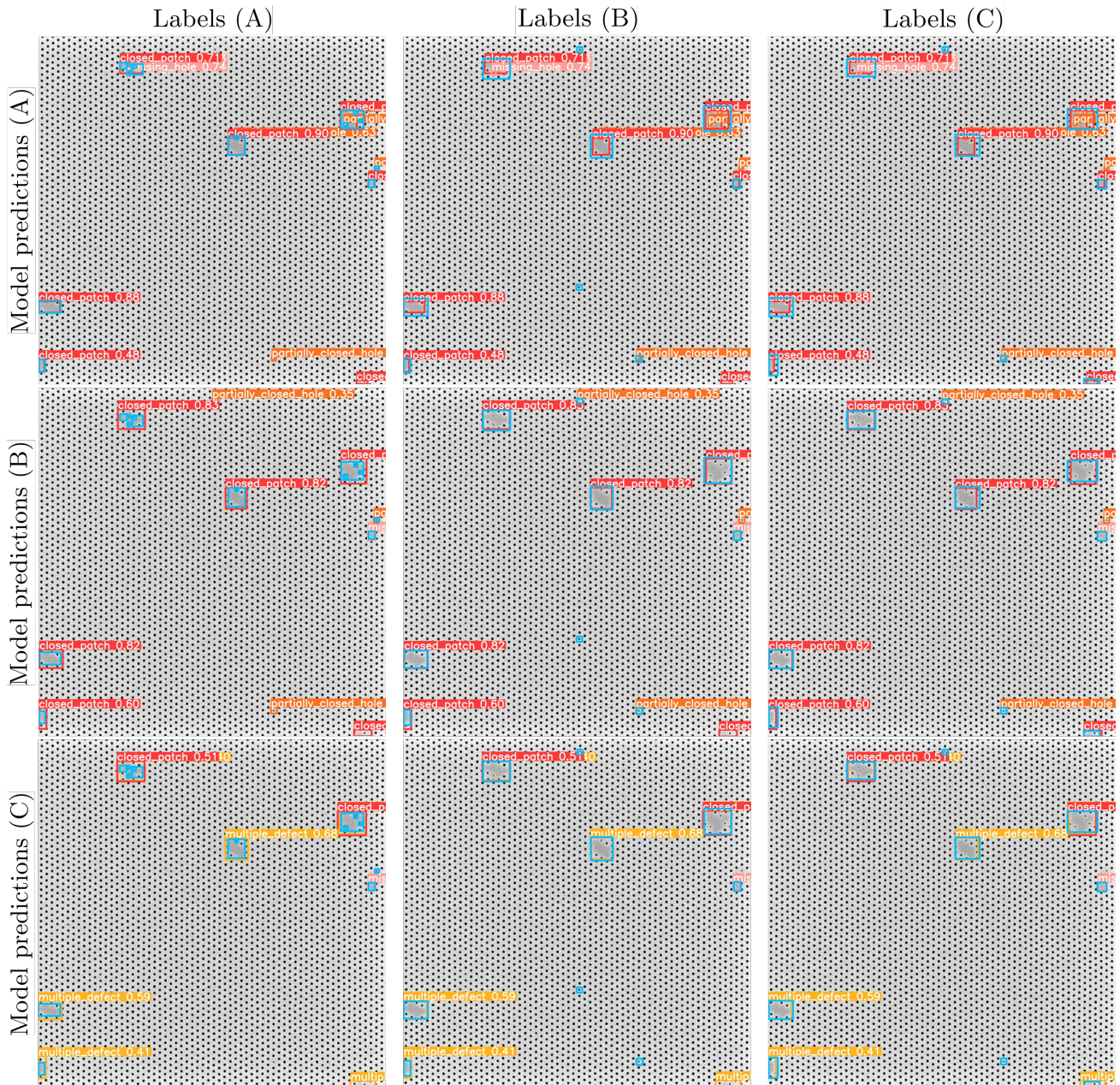


Figure 8: Prediction examples on a test image for YOLOv8m (medium) models trained on the labels from labelers A, B, and C (top row, middle row, and bottom row, respectively). Displayed predictions include confidence scores. Each prediction example is overlaid with labels of the test image from labelers A, B, and C (left column, middle column, and right column, respectively). The labels are shown in blue without class information to improve visibility. Best viewed digitally and zoomed-in for the best visibility of the prediction and label details.

Table 3: Per-class AP and mAP results for models trained and/or tested on the combined and/or final datasets. These results are the average of all YOLOv8 size variants. Post-processing refers to applying the “expert-aware post-processing” rules from Figure 2 to model predictions before comparison with test labels. Blue and red values are the best test values for combined and final data, respectively.

Dataset		AP (@0.5 IoU)			
train	test	CP	MH	PCH	All (mAP)
A	Combined	0.856	0.872	0.655	0.794
	Final	0.810	0.072	0.268	0.383
B	Combined	0.892	0.190	0.235	0.438
	Final	0.976	0.968	0.383	0.775
C	Combined	0.911	0.125	0.290	0.441
	Final	0.931	0.792	0.460	0.728
Combined	Combined	0.945	0.904	0.795	0.881
	Final	0.944	0.222	0.550	0.572
	Final (+ post-processing)	0.974	0.810	0.578	0.787
	Final (no MDs + post-processing)	0.986	0.911	0.719	0.872
Final	Final	0.977	0.984	0.797	0.919
	Final (no MDs)	0.952	0.980	0.844	0.925
Final (no MDs)	Final	0.992	0.995	0.695	0.892
	Final (no MDs)	0.995	0.984	0.853	0.944

trained on the combined dataset significantly improves the performance when tested on the final test dataset. However, this improved performance is still noticeably lower than the results obtained by the models trained on the final dataset itself. Post-prediction-processing in this manner could still be useful in a dynamic environment where new post-processing rules are regularly introduced and re-training of the model is not wanted.

6. LIMITATIONS & FUTURE WORK

In our proposed labeling combination method, we took a liberal approach to combining labels in the sense that we assume all labels are valid labels for defects. This minimizes false negatives. However, this means that any false positive labels from individual labelers will also be included in the combined dataset. This can be an issue for defects that can sometimes be similar to the background pattern such as PCH as discussed in the previous section. Future work could experiment with more conservative label combination approaches or automatic erroneous label detection and removal methods.

Another limiting assumption we make is that each image is labeled by multiple labelers. This is inefficient in the sense that a lot of duplicate work is performed, especially for labeling “obvious” defects. This could be improved in future work given access to larger datasets by (i) having different partitions of the dataset labeled only once by different labelers (see Figure 10a), (ii) training separate models on each partition (see also Figure 10a), (iii) using these models to predict pseudo-labels on the other image partitions it was not trained on (see Figure 10b), and (iv) applying a label combination algorithm on all the manual- and pseudo-labels for each image in the dataset. This allows larger datasets to be labeled using similar amounts of manual labeling effort while benefitting from the coherency and completeness of our proposed label combination method. Future work should take care to identify major labeling errors (such as the MD misclassifications by labeler C which led to poor performance even when tested on their own dataset as shown in Table 2) and ensure that each labeler labels enough images to train a model that can reliably predict pseudo-labels similar to the labeling behavior the model was trained on.

7. CONCLUSION

ML has the potential to reliably detect defects for a wide variety of patterns. This includes exploratory patterns such as HEXCH DSA patterns. However, the performance of supervised ML-based defect detection models is dependent on the quality of the labels of its training data. In this work, we proposed a method of combining

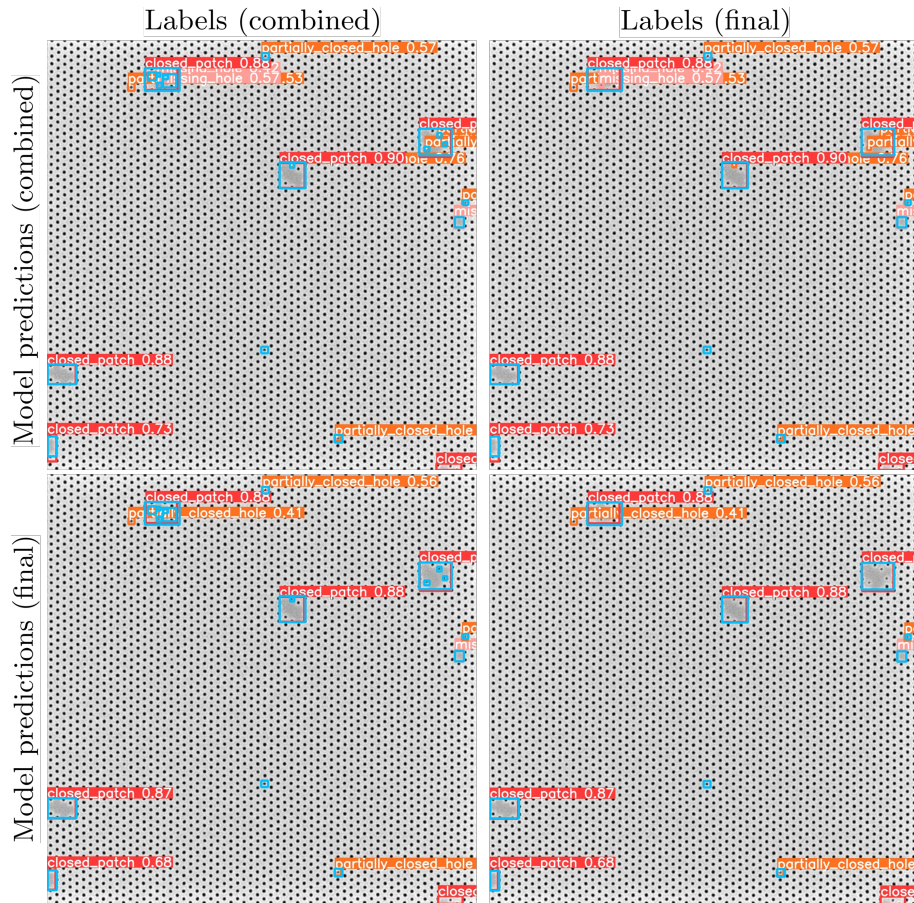
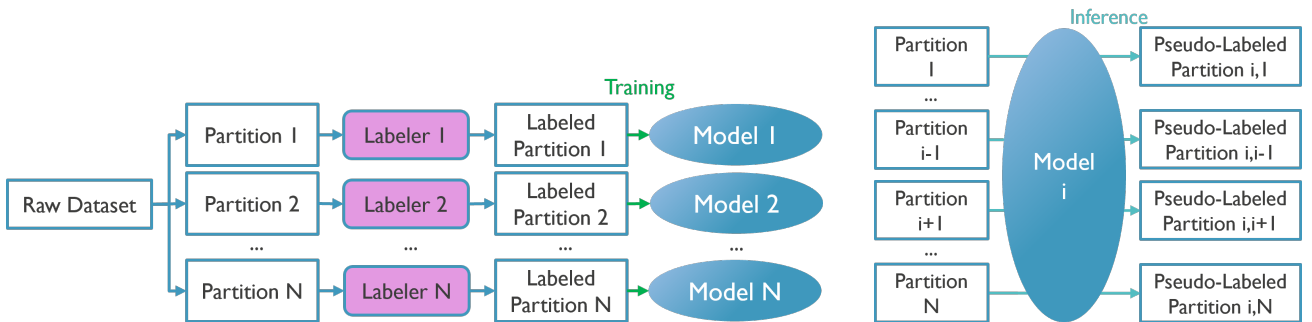


Figure 9: Prediction examples on a test image for YOLOv8m (medium) models trained on the labels from the combined and final datasets (top row and bottom row, respectively). Displayed predictions include confidence scores. Each prediction example is overlaid with labels of the test image from the combined and final datasets (left column and right column, respectively). The labels are shown in blue without class information to improve visibility. Best viewed digitally and zoomed-in for the best visibility of the prediction and label details.



(a) Per partition labeling and model training. Note each model is the same architecture but is trained on different partitions.

(b) Prediction of pseudo-labels by a model trained on labeled partition i .

Figure 10: Suggested method for semi-automated labeling of large datasets in future work.

labels from multiple human labelers to create a more coherent and complete final dataset. This final dataset best reflected the labels expected by a DSA expert without requiring exhaustive manual inspection and label correction from the DSA expert. Experimental results showed that state-of-the-art YOLOv8 models can achieve high detection precisions of more than 0.9 mAP when trained and tested on the final dataset. Finally, we suggested future work continue in the direction of data-centric ML by exploring automatic defect label removal and pseudo-label prediction.

REFERENCES

- [1] Dey, B., Goswami, D., Halder, S., Khalil, K., Leray, P., and Bayoumi, M. A., “Deep learning-based defect classification and detection in SEM images,” in [*Metrology, Inspection, and Process Control XXXVI*], Robinson, J. C. and Sendelbach, M. J., eds., SPIE (June 2022).
- [2] Redmon, J., Divvala, S., Girshick, R., and Farhadi, A., “You only look once: Unified, real-time object detection,” (2015).
- [3] Jocher, G., Chaurasia, A., and Qiu, J., “YOLOv8 by Ultralytics,” (1 2023).
- [4] Zha, D., Bhat, Z. P., Lai, K.-H., Yang, F., Jiang, Z., Zhong, S., and Hu, X., “Data-centric artificial intelligence: A survey,” (2023).
- [5] Oquab, M., Darcet, T., Moutakanni, T., Vo, H., Szafraniec, M., Khalidov, V., Fernandez, P., Haziza, D., Massa, F., El-Nouby, A., Assran, M., Ballas, N., Galuba, W., Howes, R., Huang, P.-Y., Li, S.-W., Misra, I., Rabbat, M., Sharma, V., Synnaeve, G., Xu, H., Jegou, H., Mairal, J., Labatut, P., Joulin, A., and Bojanowski, P., “Dinov2: Learning robust visual features without supervision,” (2023).
- [6] Bogatu, A., Fernandes, A. A. A., Paton, N. W., and Konstantinou, N., “Dataset discovery in data lakes,” in [*2020 IEEE 36th International Conference on Data Engineering (ICDE)*], 709–720 (2020).
- [7] Khurana, U., Samulowitz, H., and Turaga, D., “Feature engineering for predictive modeling using reinforcement learning,” in [*Proceedings of the Thirty-Second AAAI Conference on Artificial Intelligence and Thirtieth Innovative Applications of Artificial Intelligence Conference and Eighth AAAI Symposium on Educational Advances in Artificial Intelligence*], AAAI’18/IAAI’18/EAAI’18, AAAI Press (2018).
- [8] Cubuk, E. D., Zoph, B., Mané, D., Vasudevan, V., and Le, Q. V., “Autoaugment: Learning augmentation strategies from data,” in [*2019 IEEE/CVF Conference on Computer Vision and Pattern Recognition (CVPR)*], 113–123 (2019).
- [9] Ouyang, L., Wu, J., Jiang, X., Almeida, D., Wainwright, C., Mishkin, P., Zhang, C., Agarwal, S., Slama, K., Ray, A., Schulman, J., Hilton, J., Kelton, F., Miller, L., Simens, M., Askell, A., Welinder, P., Christiano, P. F., Leike, J., and Lowe, R., “Training language models to follow instructions with human feedback,” in [*Advances in Neural Information Processing Systems*], Koyejo, S., Mohamed, S., Agarwal, A., Belgrave, D., Cho, K., and Oh, A., eds., **35**, 27730–27744, Curran Associates, Inc. (2022).
- [10] Kirillov, A., Mintun, E., Ravi, N., Mao, H., Rolland, C., Gustafson, L., Xiao, T., Whitehead, S., Berg, A. C., Lo, W.-Y., Dollár, P., and Girshick, R., “Segment anything,” (2023).
- [11] Breaux, L. and Singh, B., “Automatic defect classification system for patterned semiconductor wafers,” in [*Proceedings of International Symposium on Semiconductor Manufacturing*], 68–73 (1995).
- [12] Ritchison, J. W., Ben-Porath, A., and Malocsay, E., “SEM-based ADC evaluation and integration in an advanced process fab,” in [*Metrology, Inspection, and Process Control for Microlithography XIV*], Sullivan, N. T., ed., **3998**, 258 – 268, International Society for Optics and Photonics, SPIE (2000).
- [13] McGarvey, S. and Kanezawa, M., “Automated defect review of the wafer bevel with a defect review scanning electron microscope,” in [*Metrology, Inspection, and Process Control for Microlithography XXIII*], Allgair, J. A. and Raymond, C. J., eds., **7272**, 72723N, International Society for Optics and Photonics, SPIE (2009).
- [14] Dixit, D., Green, A., Hosler, E. R., Kamineni, V., Preil, M., Keller, N., Race, J., Chun, J. S., O’Sullivan, M., Khare, P., Montgomery, W., and Diebold, A. C., “Optical critical dimension metrology for directed self-assembly assisted contact hole shrink,” *Journal of Micro/Nanolithography, MEMS, and MOEMS* **15**, 014004–014004 (March 2016). <https://www.spiedigitallibrary.org/journals/journal-of-micro-nanolithography-mems-and-moems/volume-15/issue-1/014004/Optical-critical-dimension-metrology-for-directed-self-assembly-assisted-contact/10.1117/1.JMM.15.1.014004.full> ; <https://nanolithography.spiedigitallibrary.org/article>.

[aspx?doi=10.1117/1.JMM.15.1.014004](https://doi.org/10.1117/1.JMM.15.1.014004) ; <http://ui.adsabs.harvard.edu/abs/2016JMM&M..15a4004D/abstract>.

- [15] Ito, C., Durant, S., Lange, S., Harukawa, R., Miyagi, T., Nagaswami, V., Delgadillo, P. R., Gronheid, R., and Nealey, P., “Inspection of directed self-assembly defects,” in [*Alternative Lithographic Technologies VI*], Resnick, D. J. and Bencher, C., eds., **9049**, 90492D, International Society for Optics and Photonics, SPIE (2014).
- [16] Pathangi, H., Chan, B. T., Bayana, H., Vandenbroeck, N., den Heuvel, D. V., Look, L. V., Rincon-Delgadillo, P. A., Cao, Y., Kim, J., Lin, G., Parnell, D., Nafus, K., Harukawa, R., Chikashi, I., Polli, M., D’Urzo, L., Gronheid, R., and Nealey, P. F., “Defect mitigation and root cause studies in 14 nm half-pitch chemo-epitaxy directed self-assembly LiNe flow,” *Journal of Micro/Nanolithography, MEMS, and MOEMS* **14**(3), 031204 (2015).
- [17] Cheon, S., Lee, H., Kim, C. O., and Lee, S. H., “Convolutional neural network for wafer surface defect classification and the detection of unknown defect class,” *IEEE Transactions on Semiconductor Manufacturing* **32**(2), 163–170 (2019).
- [18] Wang, Z., Yu, L., and Pu, L., “Defect simulation in SEM images using generative adversarial networks,” in [*Metrology, Inspection, and Process Control for Semiconductor Manufacturing XXXV*], Adan, O. and Robinson, J. C., eds., **11611**, 116110P, International Society for Optics and Photonics, SPIE (2021).
- [19] Dey, B., Dehaerne, E., and Halder, S., “Towards improving challenging stochastic defect detection in SEM images based on improved YOLOv5,” in [*Photomask Technology 2022*], Kasprowicz, B. S., ed., **12293**, 1229305, International Society for Optics and Photonics, SPIE (2022).
- [20] Chang, C.-Y., Chang, J.-W., and der Jeng, M., “An unsupervised self-organizing neural network for automatic semiconductor wafer defect inspection,” in [*Proceedings of the 2005 IEEE International Conference on Robotics and Automation*], 3000–3005 (2005).
- [21] Ofir, N., Yacobi, R., Granoviter, O., Levant, B., and Shtalrid, O. IEEE (oct 2022).
- [22] Dey, B., Cerbu, D., Khalil, K., Halder, S., Leray, P., Das, S., Sherazi, Y., Bayoumi, M. A., and Kim, R. H., “Unsupervised machine learning based CD-SEM image segregator for OPC and process window estimation,” in [*Design-Process-Technology Co-optimization for Manufacturability XIV*], Yuan, C.-M., ed., **11328**, 113281G, International Society for Optics and Photonics, SPIE (2020).
- [23] Dehaerne, E., Dey, B., Halder, S., and Gendt, S. D., “Optimizing YOLOv7 for semiconductor defect detection,” in [*Metrology, Inspection, and Process Control XXXVII*], Robinson, J. C. and Sendelbach, M. J., eds., **12496**, 124962D, International Society for Optics and Photonics, SPIE (2023).
- [24] Kondo, N., Harada, M., and Takagi, Y., “Efficient training for automatic defect classification by image augmentation,” in [*2018 IEEE Winter Conference on Applications of Computer Vision (WACV)*], 226–233 (2018).
- [25] Delgadillo, P. A. R., Thode, C. J., Nealey, P. F., Gronheid, R., Wu, H., Cao, Y., Neisser, M., Somervell, M. H., and Nafus, K., “Implementation of a chemo-epitaxy flow for directed self-assembly on 300-mm wafer processing equipment,” *Journal of Micro/Nanolithography, MEMS, and MOEMS* **11**(3), 031302 (2012).
- [26] Singh, A., Nam, J., Lee, J., Chan, B. T., Wu, H., Yin, J., Cao, Y., and Gronheid, R., “Manufacturability of dense hole arrays with directed self-assembly using the CHIPS flow,” in [*Alternative Lithographic Technologies VIII*], Bencher, C., ed., **9777**, 97770P, International Society for Optics and Photonics, SPIE (2016).
- [27] Doise, J., Koh, J. H., Kim, J. Y., Zhu, Q., Kinoshita, N., Suh, H. S., Delgadillo, P. R., Vandenberghe, G., Willson, C. G., and Ellison, C. J., “Strategies for increasing the rate of defect annihilation in the directed self-assembly of high- block copolymers,” *ACS Applied Materials & Interfaces* **11**(51), 48419–48427 (2019). PMID: 31752485.
- [28] Solovyev, R., Wang, W., and Gabruseva, T., “Weighted boxes fusion: Ensembling boxes from different object detection models,” *Image and Vision Computing* , 1–6 (2021).
- [29] Lin, T., “labelImg.” <https://github.com/heartexlabs/labelImg> (2021).
- [30] Brooks, J., “COCO Annotator.” <https://github.com/jsbroks/coco-annotator/> (2019).
- [31] Lin, T.-Y., Maire, M., Belongie, S., Bourdev, L., Girshick, R., Hays, J., Perona, P., Ramanan, D., Zitnick, C. L., and Dollár, P., “Microsoft coco: Common objects in context,” (2014).